Large-Scale Simulations of *a*-Si:H: The Origin of Midgap States Revisited

P. A. Khomyakov,[1] Wanda Andreoni,[1,2,3] N. D. Afify,[1,4] and Alessandro Curioni[1]

[1]*IBM Research - Zurich, Rschlikon, Switzerland*
[2]*Centre Européen de Calcul Atomique et Moléculaire (CECAM), Ecole Polytechnique Fédérale de Lausanne, Switzerland*
[3]*Institute of Theoretical Physics, Ecole Polytechnique Fédérale de Lausanne, Switzerland*
[4]*Egypt-IBM Nanotechnology Center, Cairo-Alex Desert Road, Giza, Egypt*

Large-scale classical and quantum simulations are used to generate *a*-Si:H structures. The bond-resolved density of the occupied electron states discloses the nature of microscopic defects responsible for levels in the gap. Highly strained bonds give rise to band tails and midgap states. The latter originate mainly from stretched bonds, in addition to dangling bonds, and can act as hole traps. This study provides strong evidence for photoinduced degradation (Staebler-Wronski effect) driven by strain, thus supporting recent work on *a*-Si, and sheds light on the role of hydrogen.

Since the first fabrication of solar cells based on hydrogenated amorphous silicon (*a*-Si:H) in 1976 [1], efforts devoted to improving their performance have never diminished (see, e.g., [2–7]). Photoinduced degradation of *a*-Si:H under prolonged exposure to intense light has long been known, and is generally referred to as the Staebler-Wronski effect (SWE) [8]. This is still considered one of the major disadvantages of *a*-Si:H as a photovoltaic material, leading to a decrease in the light conversion efficiency by up to 30% [7]. From its early observation to date, experimental studies have provided evidence that photodegradation is accompanied by an increase in the density of states (DOS) in the energy gap of *a*-Si:H and associate it to the presence of microscopic structural defects (see, e.g., [2–4,9]). There is no doubt that dangling bonds (DBs) generate levels in the gap, but indications exist that other metastable and likely less localized defects must also contribute to the SWE [4,10,11]. However, their nature and relevance have not been established experimentally and are still a matter of controversy. Moreover, the role of hydrogen in the SWE is unclear: on the one hand, hydrogen passivates DBs, but, on the other hand, it is believed to act as a source of DBs itself, being highly mobile under light absorption and causing bond-switching events [12–15]. A better characterization of the defect configurations contributing to photodegradation beyond DBs, and of the influence of hydrogenation is believed to help technological progress [3].

Calculations of defects in amorphous silicon, with and without hydrogenation, performed over the past three decades, were instrumental for the understanding of the physical behavior of this material (see, e.g., [16–19]). However, a step forward in the theoretical approach to the defect-SWE relation, was made only recently [20] on the basis of electronic structure calculations of a number of configurations generated for (64- or 216-atom) models of pure *a*-Si. After applying standard empirical procedures (the Wooten-Wiener-Weaire [21] process with the Keating potential [22]) to create amorphous structures, their thermodynamic stability and electronic properties were investigated within a pseudopotential density-functional theory (DFT) scheme followed by diffusion Monte Carlo (MC) computations. Configurations with highly strained bonds (SBs) were observed that had lower energy than DBs and were also able to act as deep hole traps. This interesting proposal still awaits confirmation on the relevance of ''strained-bond regions,'' not only from specific experiments but also from simulations of more realistic models and from a more extensive characterization. Moreover, a more convincing investigation should consider samples including hydrogen, a compulsory component of the amorphous silicon devices.

The study we present here responds to these open issues. Its specific aim is twofold: (i) to identify which of the many defect configurations mainly induce midgap states, thus contributing to the SWE, and (ii) to clarify the role of hydrogen. Our strategy involves, as the first step, the creation of reliable large-scale atomistic models. This implies both an accurate description of the interatomic interactions and the use of accelerated simulation methods aimed at enhancing the configuration space explored with conventional molecular dynamics (MD) or MC simulations. Therefore, samples of 500 atoms were processed with large-scale replica-exchange MD (REMD) [23] using DFT-derived classical potentials [24] and later improved with DFT-based geometry optimization. As a second step, the results of our simulations were analyzed via the bond-resolved DOS in the Wannier-functions (WF) scheme [25]. This procedure provided an unambiguous characterization of the correlation between defective bonding configurations and the DOS they induce in the gap.

We find that, contrary to the common viewpoint [2], domains with highly strained bonds significantly contribute to midgap states and not less than DBs. We also observe

that these intrinsic defects arrange in such a way as to form a network of short and long bonds through the amorphous structure, on which a hole has a high probability of localizing. Therefore, our results not only provide strong support to the conclusions of [20], but also reveal the character of the defect-related bonds participating in midgap or band-tail states. Moreover, by comparing configurations having a different amount of defects and hydrogen, the latter is shown to help reduce the strained-bond regions, provided it is kept below a certain concentration.

We considered systems of 500(Si + H) atoms in periodically repeated cubic cells with lattice constants ranging from 21.17 to 22.52 Å, for hydrogen concentrations of 5 and 10% [26]. DFT calculations [27] were performed within the pseudopotential plane-wave framework using the Perdew-Burke-Ernzerhof (PBE) [28] approximation for the exchange-correlation functional. Classical MD relied on augmented-Tersoff interatomic potentials [24] that were consistently derived from DFT-PBE results on SiONH systems with a combined energy and force fitting. In particular, these potentials were also tuned to correctly describe structures with coordination defects [24,29]. For each mass density and hydrogen content, amorphous structures were generated with a multistep procedure. First, a standard classical MD protocol (see, e.g., [17,30]) was followed, namely, melting of a c-Si sample, after random incorporation of hydrogen, and subsequent cooling of the liquid down to room temperature. Then DFT-PBE optimization of the atomic positions was performed to refine the details of the bond network. Starting from these results, the REMD [23] method was used to obtain a statistically relevant sampling of the configurational space. In particular, 128 replicas were run in the temperature range 298–1500 K for a total simulation time of 6 ns. A timestep of 2.5 fs was used and replicas were exchanged every 1.25 ps. The a-Si:H models thus obtained were validated by comparison of pair correlation functions with experimental data [26]. The final step was a further optimization of these structures in the DFT-PBE scheme.

The standard characterization of point defects (T_N) in a-Si is based on the (N-fold) coordination of the "anomalous" Si atom involved, e.g., T_3 corresponds to the presence of a DB. In our simulations, REMD produced a-Si:H models containing mainly anomalous T_4 (distorted tetrahedron) and $T_4 - T_4$ with a strained bridging Si-Si bond $(0.025/\text{Å}^3)$, and a minority of $T_3(0.0006/\text{Å}^3)$ and $T_5(0.0003/\text{Å}^3)$ [16] configurations. As expected, in spite of the strong reduction resulting from the REMD purification, the content of defects was much higher than in real annealed samples, but their persistence to REMD processing allowed us to understand their specific role.

As pointed out by several authors [18,25,31], the geometric classification is not sufficient to capture the chemical nature of the defective structures and needs to be complemented by an analysis of the electronic structure.

Wannier functions are an especially effective tool to inspect the distribution of chemical bonds. Following [25], we generated Wannier functions for several configurations randomly selected along the REMD trajectory, after DFT structural optimization. We then expanded them in terms of the Kohn-Sham eigenfunctions

$$\Psi_W^{\text{WF}}(\mathbf{x}) = \sum_i C_W(E_i)\Psi_{E_i}^{\text{KS}}(\mathbf{x}), \qquad (1)$$

where W is the center to which a single WF is ascribed (Wannier center), defined as the first minimum of the Si-WF pair correlation function, and $|C_W(E_i)|^2$ represents the projection of the density of states ($P_W\text{DOS}$) on it and can be interpreted as a bond-resolved DOS. The position of a Wannier center W helps to distinguish the different types of chemical bonds and thus discriminate the anomalous ones. Moreover, the energy-resolved $P_W\text{DOS}$ helps to identify the contribution of given bonds to the one-electron DOS. This is illustrated in Figs. 1 and 2 for samples with 5% H averaged over the last 500 exchanges of the REMD trajectory.

From the analysis of the Kohn-Sham wave functions and, in particular, of their space localization [26], we can position the top of the delocalized (band) states E_T (an estimate of the mobility edge) and thus identify valence band-tail and midgap states. This is illustrated in Fig. 1. In our PBE calculations, E_T lies at approximately 0.6 eV below the top of the occupied states E_F, which can be compared to an average band gap E_g of about 1.0 eV (~ 0.7–0.9 eV lower than experiment [32]). In particular SBs are within 0.1–0.2 eV from the DB. In order to further verify our classification of the states in the gap, we have calculated the electronic structure of the system of Fig. 1 using the HSE06 [33] xc functional that reproduces the
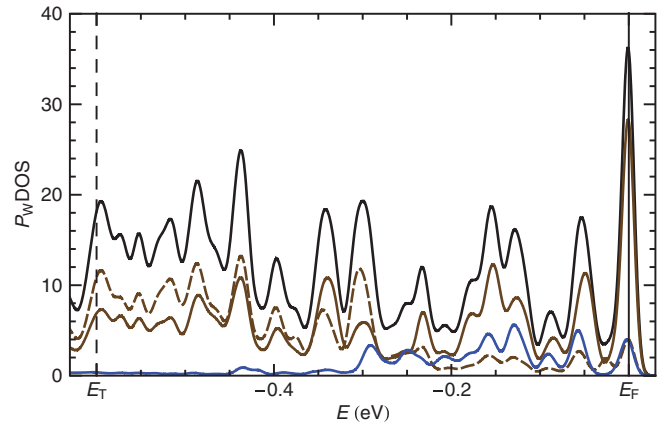
FIG. 1 (color). a-Si:H with 5% H: Density of states projected on the Wannier orbitals (Wannier centers) related to all defects (black), and analyzed in SBs [long (solid brown); short (dashed brown)] and DBs (blue). The vertical dashed line corresponds to the estimated position (see text) of the mobility edge E_T. The zero of the energy scale corresponds to the highest occupied state E_F.
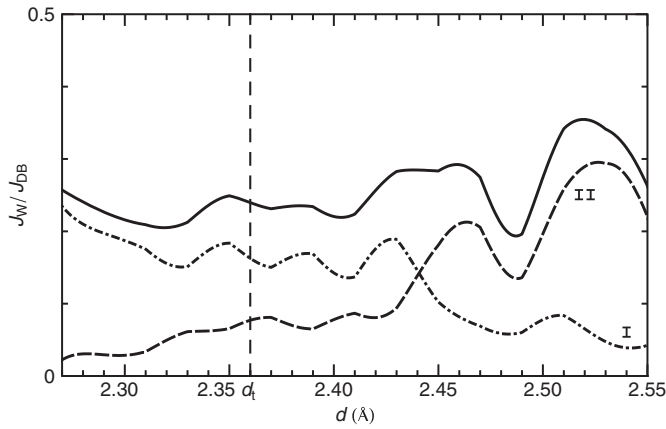
FIG. 2. a-Si:H with 5%.H: J_W (see text) relative to the DB, vs Si-Si bond length d (Å). The vertical dashed line corresponds to the average bond length d_t of the "normal" tetrahedral Si-Si bonds. The J_W integral is taken either over the whole interval (from E_T to E_F: solid line) or the lowest half (I) (dash-dotted line: $E_T - > E_F - 0.3$ eV) or the highest half (II) (dashed line: $E_T + 0.3$ eV $- > E_F$). Symbols as in Fig. 1.

FIG. 3 (color).   Spin density (shaded areas) for the a-Si:H model structure (5% H), both neutral (purple) and with a single hole (green). The network of strained bonds is shown together with the corresponding Wannier centers (filled circles). Red (green) denotes stronger (weaker) weight in the $E_T - E_F$ interval (J_W/J_{DB} larger (smaller) than 0.25).

silicon gap correctly, and repeated the same analysis based on the Wannier functions; the widening of E_g by $\sim$0.6 eV is accompanied by an analogous depletion of E_T relative to E_F, thus leaving the position of the levels associated with the coordination defects (both DBs and SBs) unaltered.

By decomposing P_WDOS in DBs and SBs (both compressed and stretched), Fig. 1 clarifies the associated energy ranges within the $E_T - E_F$ interval. DBs are fully localized in the $E_T - E_F$ interval, whereas SBs in general are not. The quantity expressing the localization of a Wannier center W within a given energy interval is clearly proportional to the integral of the P_WDOS over it. For a more significant measure of the localization in the $E_T - E_F$ interval, for each Si-Si bond length, Fig. 2 plots the statistically averaged value of this integral (J_W). In this way, SBs can be distinguished and unambiguously emerge as contributing not only to states in the band tail, as commonly believed, but also, and more importantly, to the midgap region (close to E_F). Specifically, short (compressed) bonds participate mainly in valence band tails, as observed in [34], whereas long (stretched) bonds give rise also (and especially) to midgap levels. As expected, midgap levels are also associated with DBs (Fig. 1). Therefore we can deduce that, contrary to the common belief that highly strained (long) bonds contribute only to (conduction) band tails, they are at least as important as DBs for the formation of midgap states.

In contrast to DBs, SBs are not isolated localized defects, as pointed out in previous studies [20,34], but tend to form a network (see Fig. 3). Continuous random network models [34] of a-Si exhibit uncorrelated subnetworks of short and long bonds, having different connectivity and dimensionality (3D and 1D, respectively). On the other hand, direct visual inspection of the 3D distribution of the

Wannier centers associated to SBs in our samples, reveals the presence of 1D filaments containing both short and long bonds (see, e.g., Fig. 3).

Figure 3 illustrates a typical distribution of the spin density in a neutral sample and in a positively charged one, i.e., after having removed an electron from it. In the former, although the integral vanishes over the entire space, not surprisingly we observe an accumulation of the spin density on a DB. In the latter, the spin density monitors the hole density distribution, which clearly localizes not only on the DBs but predominantly on the highly SB regions, especially those involving long bonds. This feature is common to all configurations we calculated. Therefore, our results confirm and further substantiate the proposal of a strain-driven SWE mechanism [20], in which the "highly SB domains" act as hole traps and subsequently self generate under illumination.

Our investigation also allows us to obtain insight into the role of hydrogen, which is not contained in [20]. First we remark that our simulations of the nonhydrogenated a-Si system show a stronger contribution of the stretched bonds to the density of midgap states (e.g., the integral of J_W in Fig. 2 over the range 2.40–2.55 Å increases by 42% [26]). During the REMD processing of the a-Si:H systems, we observe a strong reconstruction, leading, in particular, to configurations with a large majority of SiH bonds, and only a few SiH$_2$ in the case of 10% H. More importantly, highly strained bond regions do not contain hydrogen at equilibrium. This is consistent both with our simulations of a-Si, revealing that SBs are significantly more numerous in the

absence of hydrogen, and with experimental evidence that, in addition to passivating DBs, hydrogen dilution in *a*-Si relieves strain in the Si bond network [35]. On the other hand, both the defect concentration and the structural disorder are higher in the *a*-Si:H samples with 10% H that we have studied [26]. This suggests that beyond a critical concentration, H-doping will also significantly contribute to degradation via the structural changes and stress it induces.

In conclusion, our large-scale simulations of *a*-Si:H, combined with a detailed analysis of the bond-resolved spectrum of the occupied levels, unambiguously identified the nature of the defect structures that are responsible for valence band tails and midgap states, and for the limitation of the hole mobility. In particular, highly stretched Si-Si bonds emerge as a very important source of midgap states and hole traps, and thus as defects relevant for the SWE, at least as dangling bonds. These results reinforce previous suggestions [20] targeting the optimization of deposition processes and doping not only to reduce dangling bonds but also to release microscopic strain. Moreover, by unraveling the main role of hydrogen and the distinct contribution of compressed and stretched bonds, this work provides new and solid information, which is crucial for the tuning of the material properties controlling the performance of real devices.

[1] D. E. Carlson and C. Wronski, Appl. Phys. Lett. **28**, 671 (1976).

[2] R. A. Street, *Hydrogenated Amorphous Silicon* (Cambridge University Press, Cambridge, 1991).

[3] X. Deng and E. A. Schiff, in *Handbook of Photovoltaic Science and Engineering*, edited by A. Luque and S. Hegedus (John Wiley and Sons, Chichester, 2003), pp. 505–565.

[4] T. Shimizu *et al.*, Jpn. J. Appl. Phys. **43**, 3257 (2004).

[5] M. Zeman and J. Krc, J. Mater. Res. **23**, 889 (2008).

[6] G. R. Wronski, B. Von Roedern, and A. Kolodziej, Vacuum **82**, 1145 (2008).

[7] J. Yang and S. Guha, Proc. SPIE Int. Soc. Opt. Eng. **7409**, 74090C (2009).

[8] D. L. Staebler and C. R. Wronski, Appl. Phys. Lett. **31**, 292 (1977).

[9] A. Kołodziej, Opto-Electron. Rev. **12**, 21 (2004).

[10] T. Gotoh *et al.*, Appl. Phys. Lett. **72**, 2978 (1998).

[11] E. Stratakis *et al.*, Appl. Phys. Lett. **80**, 1734 (2002).

[12] M. Stutzmann, W. B. Jackson, and C. C. Tsai, Phys. Rev. B **32**, 23 (1985).

[13] H. M. Branz, Phys. Rev. B **59**, 5498 (1999).

[14] R. Biswas and B. C. Pan, Appl. Phys. Lett. **72**, 371 (1998).

[15] T. A. Abtew and D. A. Drabold, Phys. Rev. B **74**, 085201 (2006).

[16] S. T. Pantelides, Phys. Rev. Lett. **57**, 2979 (1986); **58**, 1344 (1987).

[17] R. Biswas, G. S. Grest, and C. M. Soukoulis, Phys. Rev. B **36**, 7437 (1987).

[18] M. Peressi *et al.*, Philos. Mag. B **80**, 515 (2000).

[19] Y.-S. Su and S. T. Pantelides, Phys. Rev. Lett. **88**, 165503 (2002).

[20] L. K. Wagner and J. C. Grossman, Phys. Rev. Lett. **101**, 265501 (2008).

[21] F. Wooten, K. Winer, and D. Weaire, Phys. Rev. Lett. **54**, 1392 (1985).

[22] P. N. Keating, Phys. Rev. **145**, 637 (1966).

[23] Y. Sugita and Y. Okamoto, Chem. Phys. Lett. **314**, 141 (1999).

[24] S. R. Billeter, *et al.*, Phys. Rev. B **73**, 155329 (2006); **79**, 169904(E) (2009).

[25] P. L. Silvestrelli *et al.*, Solid State Commun. **107**, 7 (1998).

[26] See Supplemental Material at http://link.aps.org/supplemental/10.1103/PhysRevLett.107.255502 for more details on the calculations and a description of the *a*-Si:H models.

[27] CPMD, Copyright IBM Corp. 1990–2011 and MPI für Festkörperforschung, Stuttgart, Germany, 1997–2001.

[28] J. P. Perdew, K. Burke, and M. Ernzerhof, Phys. Rev. Lett. **77**, 3865 (1996); **80**, 891 (1998).

[29] D. Fischer *et al.*, Appl. Phys. Lett. **88**, 012101 (2006); M. Ippolito *et al.*, Appl. Phys. Lett. **93**, 153109 (2008); M. Ippolito and S. Meloni, Phys. Rev. B **83**, 165209 (2011); S. Orlandini *et al.*, Phys. Rev. B **81**, 014203 (2010).

[30] K. Jarolimek *et al.*, Phys. Rev. B **79**, 155206 (2009).

[31] M. Fornari *et al.*, Europhys. Lett. **47**, 481 (1999).

[32] G. D. Cody *et al.*, Phys. Rev. Lett. **47**, 1480 (1981).

[33] J. Heyd, G. E. Scuseria, and M. Ernzernhof, J. Chem. Phys. **124**, 219906 (2006).

[34] D. A. Drabold, Y. Li, B. Cai, and M. Zhang, Phys. Rev. B **83**, 045201 (2011).

[35] J. J. Boland and G. N. Parsons, Science **256**, 1304 (1992).